

# EPJ B

Condensed Matter  
and Complex Systems

EPJ.org

your physics journal

Eur. Phys. J. B (2016) 89: 56

DOI: [10.1140/epjb/e2016-60839-6](https://doi.org/10.1140/epjb/e2016-60839-6)

## Nuclear quantum effects on the thermal expansion coefficient of hexagonal boron nitride monolayer

Florent Calvo and Yann Magnin

edp sciences



 Springer

# Nuclear quantum effects on the thermal expansion coefficient of hexagonal boron nitride monolayer

Florent Calvo<sup>1,a</sup> and Yann Magnin<sup>2</sup>

<sup>1</sup> LIPhy, Univ. Grenoble 1 and CNRS, UMR 5588, 140, Av. de la physique, 38402 St Martin D'Hères, France

<sup>2</sup> CINaM, CNRS Aix-Marseille University, Campus de Luminy, Case 913, 13288 Marseille, France

Received 22 October 2015 / Received in final form 15 January 2016

Published online 2 March 2016 – © EDP Sciences, Società Italiana di Fisica, Springer-Verlag 2016

**Abstract.** This work examines the importance of vibrational delocalization on a basic thermomechanical property of a hexagonal boron nitride monolayer, namely its thermal expansion coefficient (TEC). Using a recently parametrized bond-order potential of the Tersoff type, the TEC was theoretically obtained from the thermal variations of the lattice parameter  $a(T)$  calculated using three different methods: (i) the quasiharmonic approximation; (ii) its anharmonic improvement based on self-consistent phonons; (iii) fully anharmonic Monte Carlo simulations possibly enhanced within the path-integral framework to account for nuclear quantum effects. The results obtained with the three methods are generally consistent with one another and with other recently published data, and indicate that the TEC is negative at least up to ca. 700 K, quantum mechanical effects leading to a significant expansion by about 50% relative to the classical result. Comparison with experimental data on bulk hexagonal BN suggests significant differences, which originate from possible inaccuracies in the model that tend to underestimate the lattice parameter itself, and most likely from the 2D nature of the monolayer and the key contribution of out-of-plane modes. The effects of isotopic purity in the natural abundances of boron are found to be insignificant.

## 1 Introduction

Boron nitride can arrange at equiconcentration into a  $sp^2$  hybridized honeycomb lattice [1,2]. Monolayer hexagonal BN (h-BN) is an insulator with large bandgap close to 6 eV [3,4] whose optoelectronic properties make it a promising 2D material for transparent dielectric sheets [5,6], field-effect transistors [7] or as emitters in the deep UV regime [4]. h-BN has also been shown to resist against oxidation and friction [8], making it suitable as a coating material. In contrast to graphene, it is also free of dangling bonds [9]. Its thermal and mechanical properties have been investigated as well, notably in relation with ripple formation [10–12] but also thermal conductivity [3,13,14] which appears to be quite significant, though not as high as in graphene. The interplay between strain and electronic properties, which possibly results in the emergence of tunneling magnetoresistance [15], has been specifically addressed by Neek-Amal et al. [16], who proposed that h-BN could be further tailored as a nanosensor for gas detection.

One of the most fundamental thermomechanical properties of an extended system is the thermal expansion coefficient (TEC)  $\alpha$ , which is defined from the temperature variations of the thermally averaged lattice parameter  $a(T)$  as  $\alpha = (1/a)da/dT$ . While for a 3D material several TECs can be defined in various

crystallographic directions, for monolayers it is more relevant to focus on the in-plane coefficient. In the case of graphene, the TEC has been fairly well documented in the recent years, both theoretically [17–22] and experimentally [23–25], some controversy remaining regarding its sign and the possible temperature at which it becomes positive [26]. Undoubtedly the difficulty of synthesizing large domain graphene sheets and the necessity to disentangle from  $\alpha(T)$  the contribution of the contact and pinning regions [24,25] explain why unambiguous evaluation of the graphene TEC has remained largely elusive so far.

The present work aims to theoretically determine the in-plane thermal expansion coefficient of monolayer h-BN. Similar calculations have been reported in the very recent years, most notably by Singh et al. [12] and by Anees et al. [22], both studies being based on classical molecular dynamics (MD) simulations, and also by Sevik [21] who used the quantum mechanical quasiharmonic approximation. The results obtained from these references should be compared with caution, because the classical MD approach, although fully anharmonic, neglects nuclear quantum effects that are likely important below the Debye temperature (400 K for bulk h-BN [2]), while the quasiharmonic method essentially neglects anharmonic effects at finite temperature. In addition, the potential energy surfaces employed by these authors also differ, the electronic structure being accounted for explicitly by Sevik through density-functional theory (DFT) [21] but only implicitly

<sup>a</sup> e-mail: florent.calvo@ujf-grenoble.fr

by the groups of Singh et al. [12] and Anees et al. [22] who both used a many-body empirical potential [13] that is more appropriate for statistical simulations.

Unfortunately, there are no experimental measurements available for the TEC of h-BN *monolayers*. For the bulk (multilayer) material, the in-plane coefficient exhibits negative values of about  $-4 \times 10^{-6} \text{ K}^{-1}$  near room temperature [27–29], a value significantly overestimated in magnitude by both the quasiharmonic calculations of Sevik [21] and the classical MD results of Singh et al. [12] for the monolayer, although we note that Anees and coworkers obtained a much closer value near  $-5 \times 10^{-6} \text{ K}^{-1}$  [22]. However, the thermomechanical properties of graphene are known to differ quite a bit from those of graphite [30], and it is likely that the same conclusions carry over to hexagonal boron nitride.

In an attempt to clarify this issue, we have undertaken finite temperature calculations that account for both anharmonicities and nuclear delocalization in common footings. In addition to direct simulations in the path-integral Monte Carlo (PIMC) framework, the approach of self-consistent phonons (SCP) [31,32] was implemented as well and compared to the more basic quasiharmonic method. For the sake of consistency, the same many-body atomistic potential [13] as used by Singh et al. [12] and by Anees et al. [22] was used for the three methods, assuming quantum mechanical or classical descriptions of nuclear motion. Our results generally confirm that the TEC is negative is a broad range of temperatures, vibrational delocalization enhancing its magnitude rather significantly although values similar to those reported by Sevik et al. [13] are obtained near room temperature. Besides possibly reflecting the natural differences between mono- and multilayer h-BN, these discrepancies could originate from inaccuracies of the model, which intrinsically underestimates the lattice parameter by an amount that is comparable to pure thermal effects.

The article is organized as follows. In the next section, we describe the different methods employed to calculate the TEC from the thermally averaged lattice parameter  $a(T)$ , and emphasize some technical details regarding application of the SCP method to the numerical bond-order potential. In Section 3 we present our results and discuss them in the light of existing data, before concluding in Section 4 with summarizing remarks and some perspectives.

## 2 Methods

A complete (nonperturbative) account of anharmonicities and vibrational delocalization for a high dimensional systems requires substantial amounts of sampling of the potential energy surface, which is currently not feasible with an explicit description of electronic structure. Among existing atomistic potentials used to model boron nitride materials [33–36], the many-body bond-order potential dedicated to the h-BN monolayer and parametrized by Sevik et al. [13] to reproduce DFT calculations was thus used to perform statistically converged simulations.

### 2.1 Path-integral Monte Carlo

We have first considered the PIMC approach as a theoretically rigorous framework to compute the thermal properties of the h-BN monolayer. The PIMC method is well documented [37] and we only give here the details most relevant to the present application. Briefly, in this approach the classical particles are replaced by a set of  $P$  monomers or “beads” connected successively by harmonic springs in a cyclic fashion, the extent of this ring polymer measuring the magnitude of nuclear delocalization in the system similarly as the de Broglie thermal wavelength. In practice, for  $N$  atoms a  $N \times P$  extended system is simulated with effective potential energy

$$V_{\text{eff}}(\{\mathbf{R}_k\}) = \frac{1}{P} \sum_{k=1}^P V(\mathbf{R}_k) + \sum_{k=1}^P \sum_{\nu \in \text{atoms}} \frac{m_\nu P}{2\beta^2 \hbar^2} \|\mathbf{r}_{k,\nu} - \mathbf{r}_{k+1,\nu}\|^2, \quad (1)$$

where  $\mathbf{r}_{k,\nu} = (x_{k,\nu}, y_{k,\nu}, z_{k,\nu})$  is the position of the  $\nu$ th monomer of particle  $k$ , the cyclic condition  $\mathbf{r}_{P+1,\nu} = \mathbf{r}_{1,\nu}$  being applied for all  $\nu$ . In equation (1),  $m_\nu$  is the mass of atom  $\nu$ ,  $\beta = 1/k_B T$  with  $k_B$  the Boltzmann constant, and  $\hbar$  the reduced Planck constant. As is common in the path-integral computational framework [37], it is convenient to transform the variables  $\mathbf{r}_{k,\nu}$  into the so-called normal mode variables  $\mathbf{q}_{k,\nu}$  in such a way that the harmonic contribution to the effective potential is diagonal in those variables. Of particular relevance is then the centroid variables  $\mathbf{q}_{1,\nu} = (1/P) \sum_k \mathbf{r}_{k,\nu}$  associated with the zero eigenvalue in the diagonalization process.

At fixed temperature  $T$ , the Trotter number should be chosen large enough for path integrals to converge. In practice  $PT$  was fixed to approximately 3200 K,  $T$  being varied from 50 K ( $P = 64$ ) to 700 K ( $P = 4$ ). The PIMC simulations were carried out in the isothermal-isobaric ensemble with zero pressure, one box move being attempted every 10 atomic cycles (one cycle =  $N$  individual moves). Due to the relatively involved computational cost associated with simulating  $P$  replicas of the physical system, only a  $10 \times 10$  supercell of 200 atoms was considered,  $10^5$  MC cycles being performed at each temperature.

Classical Monte Carlo simulations ( $P = 1$ ) were also carried out for comparison, using  $10^6$  cycles per temperature in a finer grid of 25 K instead of 50 K in the quantum case. In this case, size effects could be quantified by performing some additional simulations for the  $20 \times 20$  system at selected temperatures. Such simulations could not be converged within the path-integral framework.

### 2.2 Self-consistent phonons

The method of self-consistent phonons was introduced in the 1960s to access the thermomechanical properties of anharmonic materials in a variational rather than perturbative way [31,32]. It mainly consists of replacing the true

system of reference by a set of harmonic oscillators (or phonons) approaching as best as possible the free energy of this reference system. For a periodic set of atoms, the phonon structure can be obtained from the primitive cell with all possible orientations in the Brillouin zone, or from a sufficiently large supercell but limited to a few orientations (typically the  $\Gamma$  point only). In order to compare with the Monte Carlo results, the latter description was followed by focusing on the  $10 \times 10$  supercell of 200 atoms. Under such assumption, the system of interest has  $3N - 3$  independent degrees of freedom or vibrational modes rather than a continuous set of true phonons.

In the SCP approach the free energy  $F$  of the original system (at a given and fixed lattice parameter) is evaluated using a trial harmonic Hamiltonian  $\tilde{H}$  with vibrational frequencies  $\{\omega_k\}$ ,  $k = 1, \dots, 3N - 3$ , through a variational principle based on the Gibbs-Bogoliubov inequality [38]:

$$F \leq \tilde{F} + \langle H - \tilde{H} \rangle, \quad (2)$$

where  $H$  denotes the original Hamiltonian and  $\langle \cdot \rangle$  an average on the harmonic system.  $\tilde{F}$  is the free energy of the trial harmonic system, which is obtained exactly as:

$$\tilde{F} = \langle V \rangle + \sum_k \left( \beta^{-1} \ln 2 \sinh \frac{\beta \hbar \omega_k}{2} - \frac{\hbar \omega_k}{4} \coth \frac{\beta \hbar \omega_k}{2} \right), \quad (3)$$

in which we have denoted by  $V$  the original potential of the system of interest. The thermal average  $\langle V \rangle$  of this potential over the harmonic system explicitly reads [38]:

$$\langle V \rangle = \frac{1}{\sqrt{2\pi \det \mathbf{W}}} \int V(\mathbf{R}_0 + \mathbf{R}) \exp \left( -\frac{1}{2} \mathbf{R}^\dagger \mathbf{W}^{-1} \mathbf{R} \right) d\mathbf{R}, \quad (4)$$

with  $\mathbf{R}_0$  the equilibrium configuration of the trial harmonic Hamiltonian and  $\mathbf{W}$  a thermal width matrix. The equilibrium configuration  $\mathbf{R}_0$  is determined by the conditions of vanishing gradient on all coordinates  $r_k$  as:

$$\langle \partial V / \partial r_k \rangle = -\langle f_k \rangle = 0. \quad (5)$$

To calculate the thermal width matrix we first determine the effective dynamical matrix  $\tilde{\mathbf{K}}$  such that

$$K_{ij} = \left\langle \frac{\partial^2 V}{\partial r_i \partial r_j} \right\rangle \quad (6)$$

$$\tilde{K}_{ij} = \frac{K_{ij}}{\sqrt{m_i m_j}} \quad (7)$$

which can be diagonalized into the matrix

$$\mathbf{U}^\dagger \tilde{\mathbf{K}} \mathbf{U} = \text{diag}(\omega_k^2), \quad (8)$$

and where  $\mathbf{U}$  denotes the unitary matrix that diagonalizes  $\tilde{\mathbf{K}}$ . Finally the thermal width matrix  $\mathbf{W}$  is obtained as [38]:

$$\mathbf{W} = \tilde{\mathbf{U}} \text{diag}(\rho_i) \tilde{\mathbf{U}}^\dagger \quad (9)$$

$$\tilde{U}_{ij} = \frac{U_{ij}}{\sqrt{m_i}} \quad (10)$$

$$\rho_i = \frac{\hbar}{2\omega_i} \coth \frac{\beta \hbar \omega_i}{2}, \quad (11)$$

care being taken not to include the three eigenmodes with zero eigenvalue corresponding to global translations through appropriate tagging before the diagonalization process [39].

In order to solve equations (4)–(11) self-consistently for the equilibrium position  $\mathbf{R}_0$  and the frequencies  $\{\omega_k\}$ , it is necessary to evaluate thermal averages of the first and second derivatives of the potential, which involves calculating multidimensional integrals of the kind

$$\langle A \rangle = \prod_k (2\pi\rho_k)^{1/2} \int A(\mathbf{Q}_0 + \mathbf{Q}) g(\mathbf{Q}) d\mathbf{Q}, \quad (12)$$

where we have replaced the Cartesian coordinates  $\mathbf{R}$  and  $\mathbf{R}_0$  by the normal modes  $\mathbf{Q}$  and  $\mathbf{Q}_0$ , the weighting function  $g(\mathbf{Q})$  being Gaussian for the present Harmonic potential:

$$g(\mathbf{Q}) = \exp \left( -\sum_k \frac{q_k^2}{2\rho_k} \right). \quad (13)$$

Here, and following earlier work [40], we use the Monte Carlo method with importance sampling to evaluate those integrals. We note that Errea et al. [41] have also employed stochastic integration to solve the SCP equations in a related context.

Starting from the static equilibrium position, the dynamical matrix and eigenfrequencies  $\{\omega_j\}$  are calculated, and a first simulation is performed in which the thermally averaged gradient and dynamical matrix (for the next iteration) are accumulated. From those quantities, a better approximation for the true effective equilibrium position  $\mathbf{R}_0$  is obtained by a Newton-Raphson displacement, and a new Monte Carlo simulation is performed, the process being repeated until self-consistency is reached. In particular, after each new step the eigenfrequencies change as the result of variations in the effective dynamical matrix  $\tilde{\mathbf{K}}$  of equation (7). At self-consistency, the free energy corresponding to lattice parameter  $a$  and temperature  $T$  is evaluated through equation (3). Repeating the SCP calculations by varying the lattice parameter, and minimizing the free energy as a function of  $a$  eventually yields the optimal lattice parameter as a function of temperature.

As in the case of path-integral Monte Carlo simulations, the classical limit can be straightforwardly derived from the more general quantum case, by taking  $\hbar \rightarrow 0$  in the above equations. However, contrary to the PIMC case, solving the SCP equations is computationally equivalent in both the classical and quantum mechanical descriptions.

For the present system, the numerical cost mostly originates from the Gaussian averages of the dynamical matrix, which as in the PIMC case prevents from carrying out converged calculations for systems larger than the  $10 \times 10$  supercell. At each temperature, and for each value of the lattice parameter, about 8–12 iterations were needed to numerically converge the SCP equations, the thermal averages being obtained using  $10^4$  MC cycles on the normal mode coordinates along simulations of  $10^5$  cycles. Errorbars are evaluated from the last 3 iterations of the SCP equations.

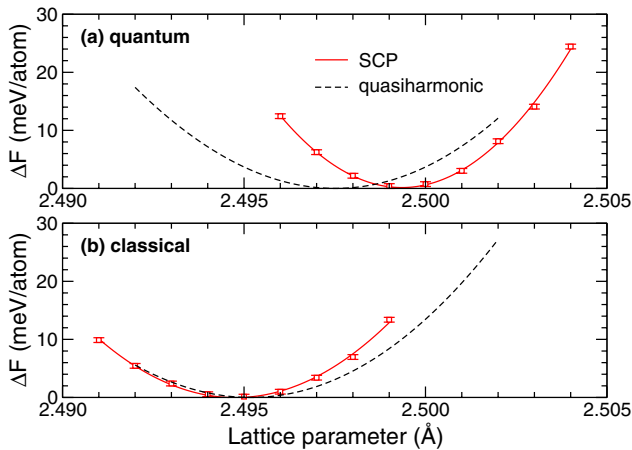


**Fig. 1.** Free energy of the h-BN monolayer at  $T = 300$  K as a function of the lattice parameter, as obtained from the quasiharmonic approximation (dashed lines) or from self-consistent phonons (red symbols interpolated as red lines). (a) Quantum mechanical description; (b) classical description.

### 2.3 Quasiharmonic approximation

At lowest order, i.e. without solving the iterative SCP equations, diagonalization of the dynamical matrix of the reference potential at the equilibrium configuration and at fixed lattice parameter  $a$  yields the harmonic free energy  $F_h(a; T)$  as a continuous function of temperature through equation (3), the thermal average  $\langle V \rangle$  being simply the static potential energy  $V_0$  at the equilibrium configuration. In this quasiharmonic approximation,  $a$  can be varied nearly continuously and  $F_h$  minimized accurately with no need to sample the energy surface or calculate multidimensional integrals.

Again, the quasiharmonic approximation can be applied in the classical regime by taking the  $\hbar \rightarrow 0$  limit in the free energy expression.

## 3 Results

The lattice parameter is directly obtained from the Monte Carlo simulations in the isothermal-isobaric ensemble. In contrast, the self-consistent phonons and quasiharmonic methods determine  $a(T)$  indirectly by minimizing approximate free energies. This procedure is illustrated in Figure 1 where the variations of  $F(a; T)$  at  $T = 300$  K obtained from both those methods are depicted in the quantum mechanical and classical descriptions of nuclear motion. The quasiharmonic results are numerically exact for the present system (supercell at the  $\Gamma$  point) and do not carry error bars. In particular, they are continuous in the ranges of lattice parameters displayed. The SCP results, however, had to be determined at discrete values of  $a$ , the free energy variations being interpolated through fourth-order polynomials from which the optimal lattice parameter was eventually obtained.

Near room temperature, vibrational delocalization leads to an increase in the lattice parameter from 2.495 Å

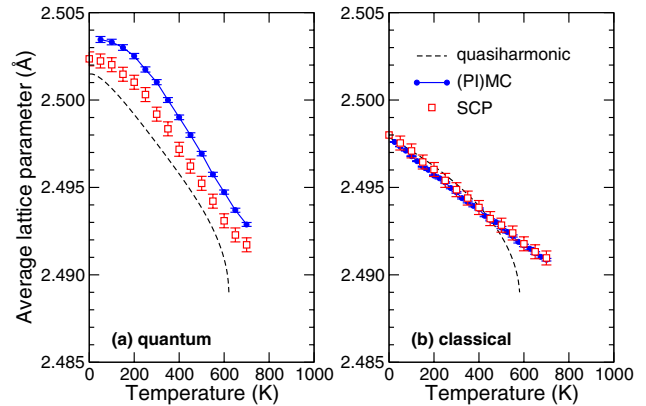


**Fig. 2.** Thermally averaged lattice parameter of the h-BN monolayer as a function of temperature, as obtained from the quasiharmonic approximation (dashed lines), Monte Carlo simulations (blue dots), or from self-consistent phonons (red squares). (a) Quantum mechanical description; (b) classical description.

to about 2.498 Å in the quasiharmonic approximation. Anharmonicities, as included in the SCP approach, further enhance this value by approximately 0.0015 Å, although the enhancement in the classical system is negligible. The larger lattice parameter in the quantum description at zero pressure is naturally expected as an expansion of the nuclear wavefunction due to zero-point vibrations. The most strongly quantum modes (bond stretches) act in the monolayer plane and contribute predominantly to the in-plane thermomechanical behavior, hence to the equilibrium lattice parameter.

Although anharmonicities are manifested on the free energies of Figure 1, the overall density of vibrational states is not strongly modified by the SCP calculations relative to the quasiharmonic results, even taking into account the slightly different lattice parameters (results not shown). These results contrast with the recent work by Errea et al. [41] on platinum, palladium and their hydrides, where the hydrogen atoms were found to be highly sensitive to anharmonicities, suppressing their mixing with the noble atoms. Here we attribute the lesser effects obtained for h-BN to its much more homogeneous vibrational nature.

Temperature contributes quite differently to  $a(T)$ , as shown in Figure 2 where the variations of this quantity with increasing  $T$ , as obtained now from the three computational methods, have been represented for the classical and quantum mechanical descriptions of nuclear motion. However, before discussing temperature effects, it is important to notice that for all calculations, the lattice parameter  $a(T)$  exhibits markedly lower values than experimental measurements for bulk hexagonal BN, the accepted range below room temperature being closer to 2.5045–2.5060 Å [27–29]. Clearly the present model (and the reference DFT calculations used for parametrizing it [13]) for the h-BN monolayer are not able to reproduce this value at such level of accuracy, although it is well possible that interplane interactions contribute to enlarging the lattice parameter of the bulk material.

In the classical case, all approaches converge to  $a = 2.498 \text{ \AA}$  at  $T = 0$ , as expected in this regime where the low-temperature limiting behavior is exactly harmonic. At finite temperature, they predict rather similar variations of the lattice parameter with temperature with essentially constant slopes, the quasiharmonic method diverging near 600 K as a signature of the emerging buckling transition that will be discussed in more details later. Overall, our results are very similar with those obtained by Anees and coworkers using the same potential, a much larger sample but at fixed surface density and with the molecular dynamics method [22]. Looking more closely into the 0–400 K range, the Monte Carlo results display marginally stronger variations than the quasiharmonic method, which is necessarily attributed to anharmonicities. The SCP method, with its partial account of anharmonicities, yields a lattice parameter in between those of the two methods, as it thus should.

For the quantum mechanical system,  $a(T)$  does not converge to the harmonic behavior even at  $T = 0$  because even the ground state wavefunction and zero-point energy are prone to anharmonicities. This is manifested by the already different zero temperature limits of the lattice parameter, which further increases from 2.5015  $\text{\AA}$  (quasiharmonic theory) to 2.5025  $\text{\AA}$  (SCP method) and nearly 2.5030  $\text{\AA}$  (PIMC simulations). The two anharmonic methods consistently predict a higher lattice parameter (by about only  $10^{-3} \text{ \AA}$  though), indicating here that anharmonicities play a greater role on vibrational delocalization than on pure thermal expansion effects. This is also consistent with the greater difference between the free energy curves obtained with the SCP and quasiharmonic methods in Figure 1 in the quantum mechanical regime relative to the classical case.

The shift of the quasiharmonic result remains at high temperatures and, as in the classical description, even increases and diverges around 600 K. At those temperatures, the quantum mechanical results with the three methods are noticeably close to their classical limits, as anticipated. However, even at 700 K the data obtained from self-consistent phonons slightly underestimate the PIMC results, which could point out once more at the approximate treatment of anharmonicities in the SCP method.

The divergence in the quasiharmonic calculations is a manifestation of the Mermin-Wagner theorem [42] stating that the long-range order in 2D crystals should be destroyed by fluctuations with long wavelengths. Such a phenomenon has been studied in details in simulations of graphene [43], and occurs here at finite temperature due to the finite size of the sample which sets a limit of the largest wavelength. Figure 3 shows in a common graph two properties illustrating the strain-induced buckling transition experienced by the h-BN monolayer as its surface density increases, namely the thickness  $\Delta z = z_{\max} - z_{\min}$  or difference between the highest and lowest atomic coordinates perpendicular to the average plane, and the lowest normal mode frequency  $\omega_{\min}$ , both obtained from the locally optimized geometry. At normal lattice parameters of the order of 2.50  $\text{\AA}$  (for the present model), the hexagonal monolayer is stable as perfectly planar ( $\Delta z = 0$ ),

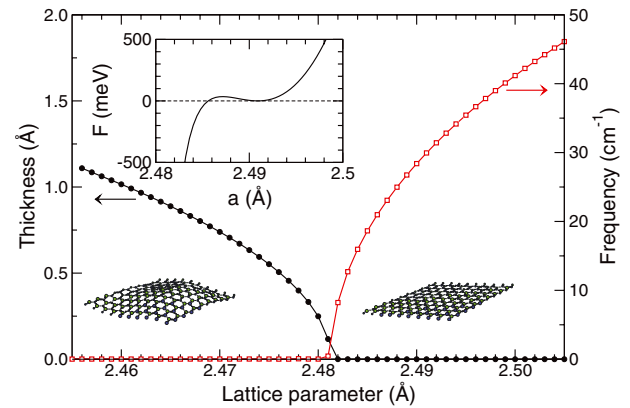


**Fig. 3.** Thickness of the h-BN monolayer (left scale) and lowest vibrational frequency (right scale) as a function of the lattice parameter. The inset highlights the variations of the quantum free energy in the quasiharmonic approximation at  $T = 600 \text{ K}$ , and the two lowest-energy structures showing both buckled and flat regimes.

with a softest mode of a few tens of wavenumbers. The free energy variations  $F(a; T)$  exhibit a single minimum along the  $a$  variable in the range  $2.48 \text{ \AA} < a < 2.51 \text{ \AA}$ , up to  $T \simeq 500 \text{ K}$ . The buckling mechanical instability takes place near  $a = 2.481 \text{ \AA}$  and is manifested by the spontaneous appearance of ripples resulting from the excitation of the imaginary frequency eigenmode in the initially flat layer. The relaxed structure is buckled with one single large ripple associated with a vanishing eigenfrequency. Such effects have been well discussed in the case of graphene [44], but also for the h-BN monolayer for which the bending rigidity causing the ripples was found to be much lower than that of graphene [12]. As the lattice parameter contracts and approaches the buckling instability, the lowering in the vibrational frequencies make the corresponding modes increasingly populated as the temperature increases. Even before the instability actually takes place, the free energies in the quasiharmonic approximation can thus become highly negative, possibly masking the physical minimum obtained at higher values of  $a$ . The (quantum) free energy obtained at  $T = 600 \text{ K}$ , shown as an inset in Figure 3, illustrates this behavior which explains why the method is no longer reliable at high temperatures, at least when performed within the supercell restricted at the  $\Gamma$  point.

In contrast, both the Monte Carlo and SCP methods naturally sample buckled configurations for all values of the lattice parameter and temperature, hence they are not so sensitive to such entropic transitions. Comparing now the high temperature limits of the three methods, we can speculate that the divergence in the harmonic free energies near the buckling transition and at those high temperatures would most likely disappear should anharmonicities be included, e.g. perturbatively [20,45].

From the thermal variations of the lattice parameter and appropriate polynomial fitting, the thermal expansion coefficient  $\alpha(T)$  was evaluated from the three methods and for classical and quantum mechanical descriptions of nuclear motion. The variations of the TEC with increasing

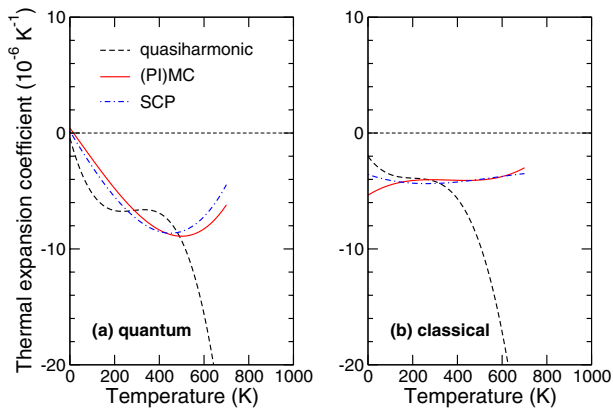


**Fig. 4.** In-plane thermal expansion coefficient obtained from polynomial fits of the lattice parameter calculated using the quasiharmonic, Monte Carlo, or self-consistent phonon approaches. (a) Quantum mechanical description; (b) classical description.

temperature are represented in Figure 4. Due to the buckling transition, the divergence in the quasiharmonic data results in an also diverging TEC above roughly 500 K. Below this temperature, the three methods predict rather similar  $a(T)$ , always negative in the temperature range considered here but with hints of a possible sign change near 800 K (quantum case) or 1000 K (classical case) upon extrapolating the SCP or MC data.

In the classical system, and consistently with the nearly linear variations of  $a(T)$ ,  $\alpha$  is approximately constant and close to  $-4 \times 10^{-6} \text{ K}^{-1}$ . The slight increase below room temperature was also noted in the MD results of Anees et al. [22]. Taking vibrational delocalization into account,  $\alpha$  vanishes as zero temperature as it should, in agreement also with experimental measurements for bulk h-BN [27–29]. Its variations up to  $T \simeq 400 \text{ K}$  are also nearly linear, the values at room temperature obtained with the three methods being close to  $-7 \times 10^{-6} \text{ K}^{-1}$  and in agreement with each other. This result is also fairly close to the quasiharmonic calculation of Sevik [21], which confirms the reliability of our supercell approach at this specific size, although we note that size effects may alter this specific conclusion (vide infra). They are also consistent with the MD data of Anees and coworkers, considering the significant differences in system size and in the computational protocol, those authors keeping the periodic box as fixed and independent of temperature [22]. Comparison with the calculation by Singh et al. [12] is more difficult because those authors obtained the TEC indirectly from the thermal variations of the bond length, rather than from the lattice parameter itself. In particular, they reported a positive value of  $\alpha$  at room temperature.

In order to clarify this possible discrepancy we have reported in Figure 5 the average nearest-neighbor B-N distance obtained from the classical and quantum Monte Carlo simulations, and its projection in the average plane. These properties are thermally averaged over configurations and, in the case of PIMC, over the various beads representing delocalized atoms. For comparison, we also show the corresponding quantities obtained from the

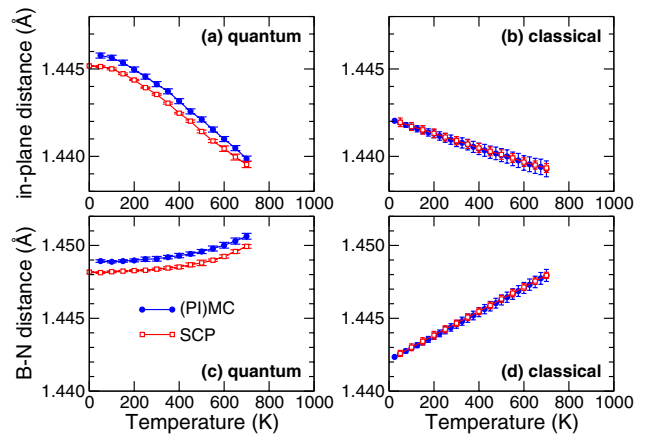


**Fig. 5.** In-plane distance (upper panels) and average distance (lower panels) between nearest neighbors obtained from Monte Carlo simulations or the self-consistent phonons method in the quantum (left panels) and classical (right panels) descriptions of nuclear motion.

last SCP iterations at the appropriate surface density that minimizes the free energy, again in the classical and quantum descriptions of nuclear motion. The two methods generally yield geometric properties in good agreement with each other that are also consistent with the variations of the lattice parameter displayed in Figure 2.

In both classical and quantum descriptions, the overall B-N distance monotonously increases with temperature, and the nearly linear variations in the classical case match the results of Singh et al. [12]. However, the in-plane distance exhibits monotonously decreasing variations with increasing temperature, a behavior which is consistent with the negative thermal expansion in these directions. In addition, the slopes match rather well those obtained in Figure 2 also when delocalization is accounted for, which confirms the values of the in-plane TEC inferred from the supercell size under the zero pressure condition. The qualitative difference in behavior between the global B-N distance and its projected value on the average plane illustrates the important role of out-of-plane modes already identified as causing the buckling transition and also related to the moderate bending rigidity of this 2D material.

Despite a reasonable agreement with other theoretical results, comparison of the TEC value with available experimental data [27–29] indicates that its magnitude is overestimated by a factor 2 at least in the case of the quantum mechanical calculations. Agreement is much better with the classical results, which are lower than the quantum mechanical values by about 40% in the 100–400 K temperature range. However this better agreement is likely to be a consequence of a compensation of errors because the behavior at low temperature is qualitatively wrong in the classical description, and furthermore the lattice parameter itself deviates from the experimental values even more than when vibrational delocalization is accounted for [27–29].

A more detailed comparison between the present results and those obtained by Anees et al. using classical MD

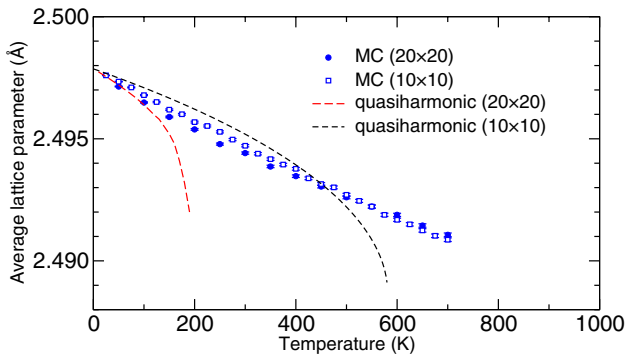


**Fig. 6.** Thermally averaged lattice parameter of h-BN monolayers as a function of temperature for two simulation supercells comprising  $10 \times 10$  or  $20 \times 20$  primitive cells, as obtained from classical Monte Carlo simulations or the quasiharmonic approximation.

suggests some residual differences, the TEC obtained by these authors at room temperature ( $-5.32 \times 10^{-6} \text{ K}^{-1}$ ) being slightly higher than the presently found classical value. In view of the much larger system size employed in this study, it is important to assess the above results against possible finite size effects of the simulation. Unfortunately, the quantum calculations in general cannot be repeated for much larger systems than those employed here, however the classical MC simulations are computationally less expensive and are convenient for discussing such issues. Figure 6 shows the thermally average in-plane lattice parameter of the h-BN monolayer obtained from the larger system having  $20 \times 20$  primitive cells through Monte Carlo simulations. The global variations of the smaller  $10 \times 10$  system are well reproduced, apart from a slightly difference curvature. Such a stronger curvature was also found by Anees et al. [22] and is indeed consistent with the marginally larger value of the classical TEC reported by these authors. However, considering the much smaller sample employed here, size effects appear relatively limited and the minor role of size effects is also supported by the very similar average B-N distance of Figure 5d in comparison with the classical results of Singh et al. [12] obtained from a large sample of nearly 38 000 atoms.

However, it is fair to notice that the quasiharmonic approximation is much more prone to finite size effects, due to the increasing role of out-of-plane modes in larger samples that due to the Mermin-Wagner theorem cause the buckling instability discussed above and illustrated in Figure 3. The predictions of the quasiharmonic model in the classical approximation  $\hbar \rightarrow 0$  for the  $20 \times 20$  system, also superimposed in Figure 6, show a much earlier divergence near 200 K instead of 600 K for the  $10 \times 10$  sample. This result indicates that the quasiharmonic method is less reliable when applied directly to supercells, and that its agreement with the other two atomistic approaches is partly fortuitous at the specific system size of  $10 \times 10$ .

The failure of the quasiharmonic model in large supercells again highlights the importance of out-of-plane modes at finite temperature, especially in the quantum case where they are more easily populated owing to their

lower frequency. Such out-of-plane modes would differ most strongly from those in the bulk (layered) material, where they would be severely hindered. This further contributes to explaining why the in-plane TEC of the bulk and monolayer systems differ so much.

Finally, and despite the important limitation on size effects noted just earlier, the quasiharmonic approach is useful to shed light on another type of nuclear quantum effect that is much more difficult to assess by direct simulation, namely that of isotopes. While all calculations reported so far in this work were performed with isotopically pure  $^{11}\text{B}$  and  $^{14}\text{N}$ , and although nitrogen is naturally nearly pure, natural boron exists in 20% proportion of  $^{10}\text{B}$ , and this isotopic heterogeneity has been shown to be responsible for the deterioration of thermal transport in bulk BN materials [46], a feature that conveys to BN nanostructures [47]. The presence of isotopes could affect the lattice parameter and the TEC through the different vibrational modes, their distributions and different contributions to zero-point motion. This effect is absent in the limit  $\hbar \rightarrow 0$ , because for a classical system the partition function factorizes into its kinetic and potential parts, the contribution of atomic masses to the free energy being purely kinetic and independent on the potential energy, hence also independent on the lattice parameter.

In order to quantify the importance of isotopic purity on the lattice parameter of h-BN and elucidate the possible contribution of such isotopic effects on the thermal expansion coefficient, the quasiharmonic calculations were repeated for the pure  $^{10}\text{B}^{14}\text{N}$  system and for the mixture containing 20% in  $^{10}\text{B}$ , using in practice the  $10 \times 10$  supercell size as the reference. In the mixture case, a random distribution of boron atom masses was imposed before evaluation of the dynamical matrix. In addition, the entire calculations were repeated over 100 independent realizations of isotopic disorder, yielding an average free energy  $\bar{F}(a; T)$  from which the optimal lattice parameter was determined as a function of temperature.

The results, depicted in Figure 7 and highlighted as an inset in the low temperature range, reveal extremely small effects hardly accessible to experimental resolution. Lighter boron leads to a global increase in  $a(T)$  by about 0.2% but no change in the TEC, the effects in the natural mixture of  $^{11}\text{B}/^{10}\text{B}$  being further reduced and barely noticeable at all. While the increase in the lattice parameter due to zero-point effects was naturally expected to be further magnified with the lighter (more quantum)  $^{10}\text{B}$  species, it was unclear whether the consequence on the overall TEC could be of significance. The present calculations thus confirm that the residual discrepancies between the present calculations and the experimental data on bulk h-BN are not caused by isotopic impurities, but rather by inaccuracies in the potential or intrinsic differences between the 2D and 3D h-BN materials.

## 4 Conclusions

Thermomechanical properties of 2D materials such as the thermal expansion coefficient are fundamental because

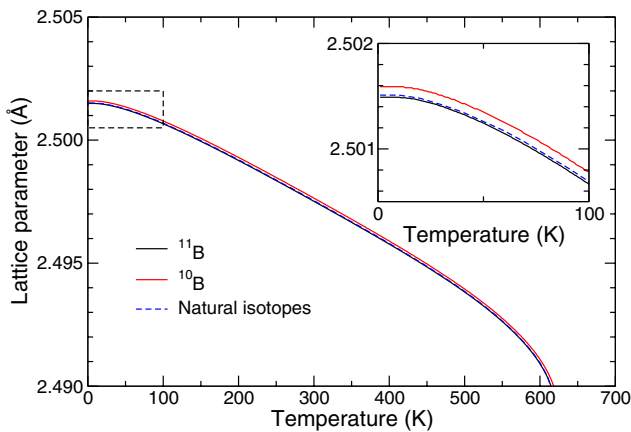


**Fig. 7.** Thermally averaged lattice parameter of the h-BN monolayer as a function of temperature obtained from the quantum mechanical quasiharmonic approximation, assuming isotopically pure  $^{11}\text{B}$  (black lines),  $^{10}\text{B}$  (red lines) or the natural mixture of 80%/20% in both isotopes (dashed blue lines).

they influence their response to different excitations. In the present work we have theoretically determined the TEC of a monolayer of hexagonal boron nitride, using a variety of computational methods that all account for nuclear quantum effects but differ in their account of anharmonicities. The results indicate that the TEC of h-BN monolayer is negative at least up to 700 K. While it is approximately constant at  $-4 \times 10^{-6} \text{ K}^{-1}$  in the classical description, quantum effects are significant, leading to more marked variations and a larger magnitude with a room temperature value close to  $-7 \times 10^{-6} \text{ K}^{-1}$ . Although our results generally agree with the recent quasiharmonic DFT calculations of Sevik [21], comparison with experimental measurements on bulk h-BN [27–29] reveals clear discrepancies in the magnitude of the TEC. Such discrepancies can be partly traced back to several causes, starting with possible inaccuracies in the atomistic potential or, of course, in the underlying DFT calculations on which the potential was fitted. Such inaccuracies are supported by the disagreement in the lattice parameter already at  $T = 0$ , which is underestimated in the model by an amount comparable to thermal effects in the 0–300 K range. Another possible contribution to the difference between the theoretical predictions and the available measurements that we could rule out is the lack of isotopic purity in boron, dedicated calculations for the natural mixture revealing barely noticeable effects.

However, the major source of discrepancy probably arises from comparing experimental data on the bulk (multilayer) material with those calculated here for the monolayer. Such a comparison is obviously not very rigorous, and the essential role of out-of-plane vibrational modes identified on various properties and previously discussed in relation with the low bending rigidity of the monolayer [12,43] should convey to intrinsic differences between the 2D and 3D materials. Besides correcting for the possible inaccuracies of the potential, it would thus be even more valuable to extend the present calculations to

bulk h-BN and determine independently the in-plane and out-of-plane lattice parameters and their associated thermal expansion coefficients. Such an extension would require further work at least in two directions, starting with the need to introduce additional terms in the atomistic potential to account for the interlayer repulsion-dispersion forces and bind the layers together. While simple Lennard-Jones pairwise interactions as proposed by Che et al. for graphite [48] would seem the most natural approach, additional difficulties could arise in h-BN owing to the unclear situation regarding stacking between layers [49]. Unfortunately, fitting such a potential based on first-principle data would also be more difficult due to the notoriously poor ability of conventional density functional methods to treat dispersion forces. Successful DFT calculations on bulk h-BN would also be required in order to clarify the possible role of interlayer interactions and temperature effects on the equilibrium lattice constant, both contributions appearing similar in magnitude according to the present calculations.

With the presently shown necessity of accounting for nuclear quantum effects, converging the PIMC or SCP calculations for the 3D materials would also be more challenging due to the larger number of simulated atoms. It is hoped that algorithmic improvements such as those recently proposed by Georgescu and Mandelshtam [50] for the SCP method could facilitate such simulations. Performing path-integral simulations on larger samples would also be clearly desirable, and in this respect it would be useful to consider the possible enhancement of such methods based on colored-noise thermostats [51].

Alternatively, it would be useful to explore other properties related to the thermal expansion coefficient, primarily the vibrational spectra. In the case of graphene, a wealth of information on the TEC comes from Raman spectroscopy [24,25,52,53], several groups notably emphasizing how this method can be used to probe defects or quantify the amount of strain [54–56]. Unfortunately, Raman spectroscopy is less practical for h-BN owing to the much lower activity of the  $E_{2g}$  mode, by a factor about 50 relative to graphene [57]. Other methods, such as grazing-incidence infrared reflection absorption spectroscopy (IRRAS), are much more promising in this respect [58]. However, as with Raman spectroscopy one expected difficulty is the production of the monolayer itself and the spectral characterization of the 2D sample, as disentangled as possible from the contribution of contact area with the support [24,25].

## Author contribution statement

All authors contributed equally to the paper.

YM gratefully acknowledges funding from European Union Seventh Framework Programme (No. FP7/2007-2013) under Grant No. 604472.

## References

- R.W. Lynch, H.G. Drickamer, *J. Chem. Phys.* **44**, 181 (1996)
- J.H. Edgar, in *Properties of Group III Nitrides*, edited by J.H. Edgar (IEE, London, 1994), p. 7
- E.K. Sichel, E.R. Miller, M.S. Abrahams, C.J. Buicchi, *Phys. Rev. B* **13**, 4607 (1976)
- K. Watanabe, T. Taniguchi, H. Kanda, *Nat. Mater.* **3**, 404 (2004)
- Y. Kubota, K. Watanabe, O. Tsuda, T. Taniguchi, *Science* **317**, 932 (2007)
- G. Kim, A.R. Jang, H.Y. Jeong, Z. Lee, D.J. Kang, H.S. Shin, *Nano Lett.* **13**, 1834 (2013)
- L. Britnell et al., *Nano Lett.* **12**, 1707 (2012)
- X. Li, J. Yin, J. Zhou, W. Guo, *Nanotechnology* **25**, 105701 (2014)
- C.R. Dean, A.F. Young, I. Meric, C. Lee, L. Wang, S. Sorgenfrei, K. Watanabe, T. Taniguchi, P. Kim, K.L. Shepard, J. Hone, *Nat. Nanotechnol.* **5**, 722 (2010)
- N. Alem, R. Erni, C. Kisielowski, M.D. Rossel, W. Gannett, A. Zettl, *Phys. Rev. B* **80**, 155425 (2009)
- K.N. Kudin, G.E. Scuseria, B.I. Yakobson, *Phys. Rev. B* **64**, 235406 (2001)
- S.K. Singh, M. Neek-Amal, S. Costamagna, F.M. Peeters, *Phys. Rev. B* **87**, 184106 (2013)
- C. Sevik, A. Kinaci, J.B. Haskins, T. Çağın, *Phys. Rev. B* **84**, 085409 (2011)
- I. Jo, T. Pettes, K. Kim, T. Watanabe, T. Taniguchi, Z. Yao, L. Shi, *Nano Lett.* **13**, 550 (2013)
- M. Hu, Z. Yu, K. Zhang, L. Sun, J. Zhong, *J. Phys. Chem. C* **115**, 8260 (2011)
- M. Neek-Amal, J. Beheshtian, A. Sadeghi, K.H. Michel, F.M. Peeters, *J. Phys. Chem. C* **117**, 13261 (2013)
- N. Mounet, N. Marzari, *Phys. Rev. B* **71**, 205214 (2005)
- M. Pozzo, D. Alfè, P. Lacovig, P. Hofmann, S. Lizzit, A. Baraldi, *Phys. Rev. Lett.* **106**, 135501 (2011)
- K.V. Zakharchenko, A. Fasolino, J.H. Los, M.I. Katsnelson, *J. Phys.: Condens. Matter* **23**, 202202 (2011)
- A.L.C. da Silva, L. Candido, J.N.T. Rabelo, G.-Q. Jai, F.M. Peeters, *Europhys. Lett.* **107**, 56004 (2014)
- C. Sevik, *Phys. Rev. B* **89**, 035422 (2014)
- P. Anees, M.C. Valsakumar, B.K. Panigrahi, *Phys. Chem. Chem. Phys.* **18**, 2672 (2016)
- W. Bao, F. Miao, Z. Chen, H. Zhang, W. Jang, C. Dames, C.N. Lau, *Nat. Nanotechnol.* **4**, 562 (2009)
- D. Yoon, Y.-W. Son, H. Cheong, *Nano Lett.* **11**, 3227 (2011)
- S. Linas, Y. Magnin, B. Poinot, O. Boisron, G.D. Förster, V. Martinez, R. Fulcrand, F. Tournus, V. Dupuis, F. Rabilloud, L. Bardotti, Z. Han, D. Kalita, V. Bouchiat, F. Calvo, *Phys. Rev. B* **91**, 075426 (2015)
- Y. Magnin, G.D. Förster, F. Rabilloud, F. Calvo, A. Zappelli, C. Bichara, *J. Phys.: Condens. Matter* **26**, 185401 (2014)
- B. Yates, M. Overy, O. Pirgon, *Philos. Mag.* **32**, 847 (1975)
- G. Belenkii, E. Salaev, R. Suleimanov, N. Abdullaev, V. Shteinshraiber, *Solid State Commun.* **53**, 967 (1985)
- W. Paszkowicz, J.B. Pelka, M. Knapp, T. Szyszko, S. Podsiadlo, *Appl. Phys. A* **75**, 431 (2002)
- D.K.L. Tsang, B.J. Marsden, S.L. Fok, G. Hall, *Carbon* **43**, 2902 (2005)
- J. Ranninger, *Phys. Rev. A* **140**, 2031 (1965)
- T.R. Koehler, *Phys. Rev. Lett.* **17**, 89 (1966)
- S.L. Mayo, B.D. Olafson, W.A. Goddard, *J. Phys. Chem.* **94**, 8897 (1990)
- A.K. Rappé, C.J. Casewit, K.S. Colwell, W.A. Goddard, W.M. Skiff, *J. Am. Chem. Soc.* **114**, 10024 (1992)
- K. Albe, W. Möller, *Comput. Mater. Sci.* **10**, 111 (1998)
- M.L. Liao, Y.C. Wang, S.P. Ju, T.W. Lien, L.F. Huang, *J. Appl. Phys.* **110**, 054310 (2011)
- D.M. Ceperley, *Rev. Mod. Phys.* **67**, 279 (1995)
- J.S. Cao, G.A. Voth, *J. Chem. Phys.* **102**, 3337 (1995)
- D.J. Wales, *Energy Landscapes* (Cambridge University Press, Cambridge, 2003)
- F. Calvo, P. Parneix, N.-T. Van-Oanh, *J. Chem. Phys.* **133**, 074303 (2010)
- I. Errea, M. Calandra, F. Mauri, *Phys. Rev. B* **89**, 064302 (2014)
- N.D. Mermin, H. Wagner, *Phys. Rev. Lett.* **17**, 1133 (1966)
- A. Fasolino, J.H. Los, M.I. Katsnelson, *Nat. Mater.* **6**, 858 (2007)
- W. Gao, R. Huang, *J. Mech. Phys. Solids* **66**, 42 (2014)
- F. Calvo, J.P.K. Doye, D.J. Wales, *J. Chem. Phys.* **115**, 9627 (2001)
- C.W. Wang, A.M. Fennimore, A. Afanasiev, D. Okawa, T. Ikuno, H. Garcia, D. Li, A. Majumdar, A. Zettl, *Phys. Rev. Lett.* **97**, 085901 (2006)
- C. Sevik, A. Kinaci, J.B. Haskins, T. Çağın, *Phys. Rev. B* **86**, 075403 (2012)
- J. Che, T. Çağın, W.A. Goddard, *Theor. Chem. Acc.* **102**, 346 (1999)
- N. Ooi, V. Rajan, J. Gottlieb, Y. Catherine, J.B. Adams, *Modell. Simul. Mater. Sci. Eng.* **14**, 515 (2006)
- I. Georgescu, V.A. Mandelshtam, *J. Chem. Phys.* **137**, 144106 (2012)
- M. Ceriotti, G. Bussi, M. Parrinello, *J. Chem. Theory Comput.* **6**, 1170 (2010)
- A.C. Ferrari, J.C. Meyer, V. Scardaci, C. Casiraghi, M. Lazzeri, F. Mauri, S. Piscanec, D. Jiang, K.S. Novoselov, S. Roth, A.K. Geim, *Phys. Rev. Lett.* **97**, 187401 (2006)
- A.C. Ferrari, D.M. Basko, *Nat. Nanotechnol.* **8**, 235 (2013)
- V. Yu, E. Whiteway, J. Maassen, M. Hilke, *Phys. Rev. B* **84**, 205407 (2011)
- J.E. Lee, G. Ahn, J. Shim, Y.S. Lee, S. Ryu, *Nat. Commun.* **3**, 1024 (2012)
- T.M.G. Mohiuddin, A. Lombardo, R.R. Nair, A. Bonetti, G. Savini, R. Jalil, N. Bonini, D.M. Basko, C. Galiotis, N. Marzari, K.S. Novoselov, A.K. Geim, A.C. Ferrari, *Phys. Rev. B* **79**, 205433 (2009)
- R.V. Gorbachev, I. Riaz, R.R. Nair, R. Jalil, L. Britnell, B.D. Belle, E.W. Hill, K.S. Novoselov, T. Watanabe, T. Taniguchi, A.K. Geim, P. Blake, *Small* **7**, 465 (2011)
- B.N. Feigelson, V.M. Bermudez, J.K. Hite, Z.R. Robinson, V.D. Wheeler, K. Sridhara, S.C. Hernández, *Nanoscale* **7**, 3694 (2015)